Effector Th1 cells alter the transcriptional output of IL-6 in acute resolving inflammation

David Millrine[*,†], Ana Cardus Figueras[*,†], Javier Uceda Fernandez[*,†], Robert Andrews[*,†], Barbara Szomolay[*,†], Benjamin C Cossins[*,†], Christopher M. Rice[#], Jasmine Li[‡], Victoria J Tyrell[*,†], Louise McLeod[§,¶], Peter Holmans[||], Valerie B O'Donnell[*,†], Philip R Taylor[*,†•], Stephen J. Turner[‡], Brendan J. Jenkins[§,¶], Gareth W Jones[#], Nicholas Topley[*], Nigel M Williams[||], & Simon A Jones[1*,†]

Affiliations –

[*]Division of Infection & Immunity, School of Medicine, Cardiff University, Cardiff, Wales, UK

[†]Systems Immunity University Research Institute, Cardiff University, Cardiff, Wales, UK

[‡]Department of Microbiology, Biomedicine Discovery Institute, Monash University, Clayton, Vitoria 3800, Australia

[§]Centre for Innate Immunity & Infectious Diseases, Hudson Institute of Medical Research, Clayton, Victoria 3168, Australia

[¶]Department of Molecular translational Science, Faculty of Medicine, Nursing & Health Sciences, Monash University, Clayton, Victoria 3800, Australia.

[||]Division of Psychological Medicine & Clinical Neuroscience, School of Medicine, Cardiff University, Cardiff, Wales, UK.

[•]UK Dementia Research Institute at Cardiff, Cardiff University, Cardiff, Wales, UK

[#]School of Cellular & Molecular Medicine, University of Bristol, Bristol, UK

[1]Corresponding author –

Professor Simon A. Jones, Division of Infection & Immunity, School of Medicine, Cardiff University, Heath Park, Cardiff, CF14 4XN, Wales, UK.

Tel: +44 29 2068 7325; Fax: +44 29 2068 7303; E-mail: JonesSA@cf.ac.uk

Abstract –

Cytokine signaling via STAT1 and STAT3 transcription factors supports and maintains tissue homeostasis. However, these signals also promote inflammation-induced tissue injury. To understand how these inflammatory outcomes are shaped, we applied RNA-seq, ChIP-seq, and ATAC-seq to identify the transcriptional output of STAT1 and STAT3 in peritoneal tissues during acute resolving inflammation and inflammation primed to drive fibrosis. Bioinformatics focussed on the transcriptional output of IL-6 in both settings and examined how pro-fibrotic IFNγ-secreting $CD4^+$ T-cells altered the interpretation of STAT1 and STAT3 cytokine cues. In acute resolving inflammation, STAT1 and STAT3 cooperated to drive stromal gene expression affecting anti-microbial immunity and tissue homeostasis. Introduction of IFNγ-secreting $CD4^+$ T-cells altered this transcriptional program and channeled STAT1 and STAT3 to a previously latent GAS motif in *Alu*-like enhancer sequences. STAT1 and STAT3 binding to this conserved sequence revealed evidence of reciprocal cross-regulation. Genes affiliated with these loci included those involved in pathophysiology. Thus, effector T-cells re-tune the transcriptional output of IL-6 by shaping a regulatory interplay between STAT1 and STAT3 in inflammation.

Key words –

Cytokines, Inflammation, Fibrosis, Transcription Factors, Enhancers, Retrotransposons

Introduction –

Cytokines are essential for development, tissue homeostasis, and the regulation of inflammation (1). The intracellular signaling pathways controlling these activities are intrinsically linked, and aberrant host defense compromises tissue integrity and physiological function. Patients treated with anti-cytokine therapies often provide evidence of this relationship (2). For example, inhibitors of interleukin (IL)-6 show less efficacy in diseases where IL-6 maintains tissue homeostasis and barrier immunity (3-10). It is unclear how IL-6 operates through a single receptor signaling cassette to deliver normal physiology and the transition to tissue injury and pathophysiology.

Interleukin-6 receptor signaling involves activation of Janus kinases (Jak) and members of the Signal Transducer and Activator of Transcription (STAT) family (3, 6). The Jak-STAT pathway senses and interprets environmental cues essential for proliferation, survival, and functional identity (11). Interleukin-6 regulates gene expression through the transcription factors STAT1 and STAT3 (11-17). These proteins share a complex regulatory interplay, and gene ablation studies show that STAT1 and STAT3 often counteract each other or engage shared enhancers(3, 18, 19). These interactions re-tune the interpretation of cytokine cues and instruct alternate patterns of gene regulation (14, 16, 20-26).

Resident tissue cells respond to immune challenges by steering decision-making processes that affect the course of inflammation (1, 27-29). These activities rely on a cytokine network that promotes communication between stromal tissue and infiltrating leukocytes (29). For example, IL-6 is a major determinant of disease outcome in peritonitis and directs anti-microbial immunity and the resolution of inflammation (30-35). However, this IL-6 response becomes compromised following repeated immune activation and transitions acute inflammation towards a more pro-fibrotic environment (21). Here, peritoneal increases in Th1 cell numbers and associated IFNγ signaling *via* STAT1 promote tissue injury and remodeling (21). How this increase in STAT1 activity affects the interpretation of STAT3 signals is unknown. Here, we have used next-generation sequencing methods to compare the transcriptional properties of STAT1 and STAT3 in acute peritonitis in the presence or absence of Th1 cells. Our analysis shows that IFNγ-secreting T-cells shape the transcriptional output of IL-6 by establishing a dynamic regulatory interplay between STAT1 and STAT3.

Results –

Effector Th1 cells shape stromal responses to peritonitis– The transition of acute resolving peritonitis to inflammation-induced tissue injury requires the expansion of pro-fibrotic Th1 cells in response to repeated inflammatory activation (21, 33, 36). How these cells impact the stromal tissue response to peritonitis remains largely unknown (21, 34, 35, 37). We, therefore, challenged (i.p) mice with a cell-free supernatant from *Staphylococcus epidermidis* (SES). Mice receiving SES were also co-administered with naïve $CD4^+$ T-cells, or $CD4^+$ T cells expanded *ex vivo* into pro-fibrotic Th1 cells. In a parallel approach, mice also received naïve $CD4^+$ T-cells, or $CD4^+$ T-cells expanded *ex vivo* into Th1 cells (normalized to 10^6 IFNγ-secreting T-cells) (21). At 3 and 6 hours, we harvested tissues from the peritoneum for RNA-seq. K-means clustering was restricted to transcripts significantly regulated above baseline following the SES challenge (Log2FC>1.75, P_{adj}<0.05). The administration of naive $CD4^+$ T-cells acted as further control for mice receiving SES and Th1 cells (SES+Th1) (**Fig-1A**). Applying statistical tools (silhouette, gap statistics, and elbow), we identified four clusters of gene regulation in the datasets from mice challenged with SES alone or SES+Th1 (**Fig-1B,** Supplemental Figure-1). We observed 821 differentially regulated transcripts whose expression altered in at least one of the experimental conditions. SES challenge regulated a total of 225 genes, with the activities of Th1 cells affecting another 673 genes. Genes mapped to each cluster revealed biological activities associated with Jak-STAT cytokine signaling (**Fig-1C**). These include genes affecting vascularization, epithelial morphogenesis, and hyperplasia (e.g., *Angpt4*, *Egr3*, *Igfbp2*, *Ntf3*, *Tbxa2r*). Others share involvement in innate sensing pathways (e.g., *Ifitm1*, *Marco*, *Myd88*) and leukocyte infiltration (e.g., *Ccl3*, *Ccl5*, *Ccl2*, *Cxcl1*, *Cxcl10*, *Icam1*, *Vcam1*). The presence of Th1 cells altered gene expression within each of these clusters, with gene set analysis revealing enrichment of pathways attributed to IFNγ signaling (e.g., *Ido1, Irf1*, *Mxd1*, *Stat1*). These include activities that compromise tissue integrity and others responsible for host immunity.

Th1 cells modify the inflammatory output of IL-6– Previous studies have showcased the importance of IL-6 in SES-induced inflammation and identified a potential functional synergy between IL-6 and IFNγ (21, 33, 38, 39). We, therefore, quantified IL-6 and sIL-6R levels in peritoneal lavage from mice challenged with SES in combination with naïve $CD4^+$ T-cells or Th1 cells. SES administration promoted a rapid yet transient increase in IL-6 (Supplemental Figure-2). While

physiological levels of IFNγ remained below detection limits in mice treated with SES and naïve $CD4^+$ T-cells, the presence of Th1 cells increased peritoneal IFNγ (Supplemental Figure-2). This increase was associated with enhanced IL-6 and sIL-6R production. Thus, IFNγ has a positive impact on the availability and bioactivity of IL-6 during acute resolving inflammation. To establish whether this relationship altered the transcriptional output of IL-6, we performed RNA-seq on peritoneal tissues obtained from SES challenged wild type (*wt*) and *Il6*$^{-/-}$ mice. Following K-means clustering, we identified 241 transcripts displaying a significant difference (Log2FC>1.75, P_{adj}<0.05) between wt and *Il6*$^{-/-}$ mice (**Fig-2A** & **Fig-2B**, Supplemental Figure-2). Genes under IL-6 regulation included those involved in cellular functions essential for tissue homeostasis and architecture (e.g., *Atoh1*, *Cldn5*, *Fgfbp1*, *Npnt*, *Otog*, *Oxtr*, *Pdx1*, *Pgr*, *Stab2*). Other examples revealed roles in host defense (e.g., *Trim52*, *C7*, *Scube*1), leukocyte recruitment (e.g., *Ccl8*, *Ccl17*, *Ccl22*, *Ccl24*), and cell adhesion (e.g., *Selp*, *Adgrb2*) (**Fig-2C,** Supplemental Figure-1). Based on these latter observations, we developed a flow cytometric method to establish the role of IL-6 in coordinating anti-microbial host responses. Briefly, we exposed neutrophils loaded with the peroxidase substrate 3'(p-aminophenyl) fluorescein (APF) to serum optimized Staphylococcus epidermidis labeled with DDAO-far-red. Comparing the effector properties of circulating Ly-$6B^{hi}$ Ly-$6G^{hi}$ neutrophils from *wt* and *Il6*$^{-/-}$ mice, we saw no differences in phagocytosis or respiratory burst (Supplemental Figure-2). However, infiltrating neutrophils from *Il6*$^{-/-}$ mice treated (i.p.) with $5x10^8$ cfu DDAO-far-red labeled *Staphylococcus epidermidis* showed reduced neutrophil responses (**Fig-2D**, Supplemental Figure-2). We substantiated these findings by visualizing fluorescent bacteria in neutrophils using imaging flow cytometry (Supplemental Figure-2). Since IL-6 requires sIL-6R to regulate stromal responses within the peritoneal cavity, we conducted an identical experiment in *wt* mice treated with the IL-6 trans-signaling antagonist soluble gp130 (sgp130). Treatment with sgp130 significantly reduced the effector properties of infiltrating neutrophils in infected mice (**Fig-2D**). Moreover, by reconstituting IL-6 signaling through the administration (i.p.) of a chimeric IL-6-sIL-6R fusion protein (HDS), we could correct this functional defect (**Fig-2D**, Supplemental Figure-2). Thus, IL-6 governs neutrophil responses to local infection.

Th1 cells shape activities of STAT1 and STAT3 transcription factors– STAT transcription factors become rapidly activated following SES challenge (Supplemental Figure-3), with maximal activation

coinciding with the 3 and 6 hours chosen for our RNA-seq analysis (21, 35, 37). Significantly, STAT1 activities often shape the transcriptional output of IL-6 and STAT3 (11, 15, 16, 40). To examine this relationship in SES inflammation, we extracted peritoneal tissues from challenged *gp130*$^{Y757F:Y757F}$ mice with SES. These animals possess a single tyrosine-to-phenylalanine substitution in the cytoplasmic domain of gp130 that prevents the negative regulation of STAT1 and STAT3 following cytokine activation (35, 36). Immunoblot for tyrosine-phosphorylated STAT1 (pY-STAT1) and STAT3 (pY-STAT3) showed that SES triggers a prolonged activation of both transcription factors in these mice (**Supplemental Figure-3**). Moreover, partial *Stat3* ablation in *gp130*$^{Y757F:Y757F}$ mice (*gp130*$^{Y757F:Y757F}$:*Stat3*$^{+/-}$) extended the duration of pY-STAT1 activity following SES challenge (**Supplemental Figure-3**). Thus STAT1 and STAT3 activities are interlinked in SES inflammation and may explain how Th1 cells impact the transcriptional output of IL-6. We, therefore, applied chromatin immunoprecipitation-sequencing (ChIP seq) to investigate STAT1 and STAT3 transcription factor binding following SES challenge (**Fig-3**). Our analysis identified sequencing peaks displaying a four-fold enrichment above input (P<0.0001; false discovery rate 0.05). These mapped to transcriptional start sites (TSS), exons, introns, and intergenic regions (**Supplemental Figure-3**). Motif enrichment analysis (MEME-ChIP) confirmed the specificity of these interactions and identified consensus DNA binding motifs for STAT1 or STAT3 beneath the mapped sequencing peaks (**Supplemental Figure-3**).

We next explored how these transcription factors interact with the genome by comparing STAT1 and STAT3 binding to DNA extracts from mice challenged with SES or SES+Th1 cells. STAT transcription factor binding was noticeably different in both treatment groups (**Fig-3**; **Supplemental Figure-3**). Following SES stimulation STAT1 and STAT3 worked in close partnership. The introduction of Th1 cells increased the number of sequencing peaks identified by ChIP-seq (**Supplemental Figure-3**). This increase in STAT1 and STAT3 binding sites corresponded with the enhanced gene regulation associated with the presence of Th1 cells and included genes expressed by mesothelial and fibroblast populations (**Fig-1 & Fig-2**; **Supplemental Figure-3**). Comparing the binding of STAT1 and STAT3 in genomic extracts from *wt* and *Il6*$^{-/-}$ mice, we also noted evidence of transcription factor cross-regulation at these sites. While STAT transcription factors often bound similar genomic coordinates, *Il6* deficiency influenced the preference for STAT1 or STAT3 binding at these loci (**Fig-**

3B). The deletion of *Il6* frequently resulted in a loss of STAT3 binding but a corresponding increase in STAT1 binding at distal sites downstream of the TSS. This is reflected in pairwise comparison of transcription factor binding coordinates that support reciprocal STAT1 and STAT3 binding patterns in wt and *Il6*$^{-/-}$ mice at locations bound by P300 in the SES+Th1 condition (**Supplemental Figure-3**). Genes displaying this form of cross-regulation identify involvements in cytoskeletal organization (e.g., *Mtus2*, *Actb*), Rho signaling (e.g., *Rhpn2, Wasf1*), metabolism (e.g., *Angptl4*, *Mtor*, *Neu2*, *Pgm1*), and tissue remodeling (e.g., *Timp1*, *Col2a1*, *Vegf*). At the transcriptional level, this switch from STAT3 to STAT1 coincided with changes in gene regulation that impacted the induction or suppression of gene activity under *Il6* deficiency (**Supplemental Figure-3**). These included suppression of genes affecting cellular differentiation (e.g., *Dnaic1*, *Eif2s3y*), and increases in genes linked with matrix protein biosynthesis (e.g., *Acan*, *Npnt*, *Col2a1*). Thus, STAT1 and STAT3 differentially impact processes affecting tissue homeostasis.

The alternate patterns of STAT1 and STAT3 binding identified by ChIP-seq suggested that these interactions may control different transcriptional outcomes. To understand this dynamic, we first used Assay for Transposase-Accessible Chromatin-sequencing (ATAC-seq) to establish whether differences in STAT transcription factor binding was impacted by changes in chromatin accessibility. The heatmap profile shows chromatin accessibility across the entire genome for both *wt* and *Il6*$^{-/-}$ mice following challenge with SES+Th1 cells (**Fig-4A**). Differential binding analysis (*Diffbind*) of ATAC-seq datasets identified chromatin regions regulated by IL-6. These regions were predominantly located in and around TSS (**Fig-4B, Fig-4C**). Motif enrichment analysis of the DNA sequences aligned to these peaks identified concensus sites for STAT and IRF transcription factors, and included others (e.g., KLF15, NRF1, HOXOA13 and several zinc-binding factors) linked with tissue homeostasis and epigentic modifications (**Fig-4D**). Access to these sites was partially restricted by the absence of *Il6*, which suggests that IL-6 promotes chromatin remodelling during inflammation (**Fig-4C**).

STAT transcription factors recognize discrete enhancer elements– The proximity of STAT1 and STAT3 binding sites to consensus sequences for other transcription factors suggested links to hyperactive regulatory regions such as super-enhancers. We, therefore, mapped the genomic localization of P300 in peritoneal tissue extracts from mice challenged with SES+Th1 cells (**Fig-5A**).

This histone acetyltransferase controls chromatin remodeling and often localizes active or poised enhancers, where P300 functions as a scaffolding factor and co-regulator of transcription factor activity (11, 41). ChIP-seq analysis for P300 identified sequencing peaks sharing STAT transcription factor binding (**Supplemental Figure-3**). However, P300 mapping represented a small proportion (<11%) of the total sequencing peaks identified for STAT1 and STAT3 (**Fig-5A**). Although 60% of the P300 loci showed a switch in STAT transcription factor binding under Il6 deficiency, these changes were more prominent at loci lacking P300 (**Fig-5A**). Examples included genes encoding *Stat6*, *Adamts1*, *Socs1*, and interferon regulated genes including *Irf1*, *Irf9, Mx2*, *Il15*, and *Ifit1*. These loci showed significant association with STAT3 binding in samples from *wt* mice (**Fig-5A**). In contrast, ChIP-seq datasets from *Il6*$^{-/-}$ mice showed an increased preference for STAT1 binding at these sites. A small number of genomic loci displayed both STAT1 and STAT3 binding (**Fig-3C**, **Fig-5A**).

We next performed a motif analysis of the sequencing peaks identified by ChIP-seq to reveal enhancer sites linked with STAT1 and STAT3 binding (**Supplemental Figure-3**). Combining the datasets from *wt* and *Il6*$^{-/-}$ mice, we identified a centrally enriched motif with 90-95% sequence identity (CCTGTAATCCCAGC) to previously annotated GAS elements (MA0137.3, MA0144.2) (**Fig-5B**). Given the conserved nature of this sequence within the datasets, we used coordinate mapping of the murine genome to identify gene loci containing the CCTGTAATCCCAGC motif. These extended sequences possessed specific genomic architectures that resemble a family of Short Interspersed Nuclear Elements (SINE) classified as *Alu*-like elements (**Fig-6**), which coordinate long distance chromatin rearrangements through defined transcriptional mechanisms(42). We, therefore, mapped the annotation of our next-generation sequencing peaks against the coordinates of known interspersed repeats and low complexity DNA sequences generated through the RepeatMasker bioinformatic package. Our analysis supported the interaction of STAT1 and STAT3 with a subset of SINE known as *Alu*-like B1 elements (**Fig-6A**). *Alu*-like elements possess conserved regulatory motifs. The CCTGTAATCCCAGC site resided close to a Pol-II A-box, located at the 5' end of the extended 100-150bp sequence and was flanked by sequence motifs for T-bet and Runx3 (**Fig-6B**). STAT transcription factor binding to *Alu*-like B1 elements was a central feature of DNA from mice challenged with SES and Th1 cells (**Fig-6A**). Thus, the activities of Th1 cells channel STAT1 and STAT3 towards enhancers that remained idol in acute SES activation.

The Alu associated GAS-like motif defines immune signaling pathways linked to human physiology– Based on the sequence homology between murine and human Alu elements, we assessed whether the GAS-like sequence (GAS-Alu motif) correlated with single nucleotide polymorphisms (SNP) in human disease (**Fig-7A**). From publicly available genome-wide association studies (GWAS), we identified GAS-Alu motifs in enhancer sequences designated by the Fantom5 consortium. Our analysis revealed 8423 sequences, mapping to 2334 genes (Entrez) (Supplemental Figure-5). Genes affiliated with the GAS-Alu motif contributed to various processes affecting immune cell regulation. Some act as intermediates involved in thrombopoietin (e.g., *PRKCB*), VEGF (e.g., *PDGFC*, *ACTG2*), and integrin (e.g., *RAPGEF1*) signaling. Others regulate leukocyte signaling (e.g., *VAV1*, *CACNG3*, *PPP3CB*) and migration (*ARHGAP8*, *ACTG2*), or tissue turnover (e.g., *MYO10*, *ARHGEF19*). These included several mapped by our ChIP-seq analysis of murine STAT1 and STAT3. For example, *ARHGEF19* (*Arhgef19*), *COL5A* (*Col5a*), *MYO10* (*Myo10*), *PPARG* (*Pparg*), *PRKCB* (*Prkcb*), and *RABGEF1* (*Rabgef1*).

Next, we downloaded GWAS summary statistics (n=2505) hosted by major repositories (NHGRI-EBI, CTGLab, NCBI). Magma analysis was performed on Fantom5 linked gene sets and hallmark signatures of IL-6 and IFNγ activity downloaded from msigdb (Broad Institute). These were compared to a series of randomized and shuffled gene lists. Genes aligned to the HLA locus were excluded from our datasets to control against the high degree of linkage disequilibrium at these loci. Magma output files were screened using enhancers mapped by the FANTOM5 project to identify 257 GWAS displaying enrichment of the GAS-Alu motif (Supplemental Figure-5). Pairwise comparison (Pearson) and hierarchical clustering of these GWAS datasets identified three clusters based on gene identity (**Fig-7A**). Genes affiliated with Cluster-2 were linked to various immunological processes and involvements in pathophysiology (**Fig-7B**). They also exhibited a high degree of enrichment with IL-6 and IFNγ gene signatures identified by FANTOM5. Thus, the GAS-Alu motif classifies examples of Jak-STAT cytokine signalling in immune pathology.

Discussion –

Cytokines are regulators of inflammation and control transcriptional processes that instruct both the provision of competent host defense and the development of inflammation-induced tissue injury (43, 44). Studies in bacterial peritonitis reveal that IL-6 and IFNγ are critical determinants of disease outcome (4, 10, 21, 27, 31-33, 35, 36, 38, 39, 45-47). Interleukin-6 compromises tissue repair by supporting the expansion of pro-fibrotic IFNγ-secreting $CD4^+$ T-cells as a response to repeat resolving inflammation (21). While these cytokines rely on STAT1 and STAT3 signaling (21, 35-37), it is currently unclear how these transcription factors instruct changes in gene expression to instruct anti-microbial host immunity, tissue scarring, and fibrosis. Through a detailed analysis of STAT1 and STAT3 activities in peritoneal tissues following inflammatory challenge, we now report that IFNγ-secreting $CD4^+$ T-cells re-tune the transcriptional output of IL-6.

Control of Jak-STAT signaling is complex and includes a regulatory interplay between individual STAT transcription factors (11, 12, 14, 15, 45, 48-51). For example, patients with *STAT1* gain-of-function or *STAT3* loss-of-function mutations often display similar clinical features. These include increased susceptibility to infections at barrier surfaces, eczema-type rashes, and bowel perforations (51-57). These clinical phenotypes also present in patients lacking *IL6R* or mice lacking *Il6* and often reflect the importance of STAT3 in governing innate immunity (58-64). Our analysis showed that IL-6 controls stromal activities that enhance the phagocytic properties of infiltrating neutrophils. Collectively, these data support the importance of STAT1 and STAT3 cross-regulation in determining the course of disease outcome.

Genomic loci mapped by the histone acetyltransferase P300 provide an accurate means to identify tissue-specific enhancers and their associated properties (65, 66). For example, P300 binding often identifies genes linked with regulatory networks affecting autoimmunity and T-cell effector function (18, 40, 67). These include interactions with STAT transcription factors (68). Our analysis revealed very few P300 sites linked with STAT1 and STAT3. Instead, the presence of Th1 cells led to an unveiling of alternate enhancer sites populated by STAT1 or STAT3. Genes affiliated with these loci contribute to tissue remodelling, fibrosis, solute transport, membrane permeability, and hypoxia. Thus, our data support ideas for an agonist-specific repertoire of latent enhancers employed to sense and interpret changes in the tissue microenvironment (69). For example, studies in

macrophages have shown that transcription factors linked with myeloid cell development (e.g., the ETS-domain transcription factor PU.1) often shape the way transcription factors (e.g., NF-κB, AP-1, interferon response factors) engage the genome (70). Thus, our analysis endorses theories that genes with similar biological functions share common transcriptional mechanisms (71).

Evaluation of the DNA motifs bound by STAT1 or STAT3 in peritoneal tissue from mice receiving SES and Th1 cells showed sequence homology with *Alu*-like repeats commonly described as short interspersed nuclear elements (72, 73). These sequences are highly abundant in the genome of mice and humans and contribute to the control of non-allelic recombination (e.g., duplications or deletions of DNA segments), polyadenylation, splicing processes, and the transcription of gene-rich regions (73, 74). Importantly, *Alu* sequences often display variations in the level of DNA methylation and possess multiple transcription factor binding sites that infer a dynamic influence on gene regulation (75, 76). Our analysis showed that IL-6 signaling, in association with IFNγ-secreting Th1 cells, promotes STAT3 binding to *Alu* sequences. This switch in transcriptional control resembles cytokine responses in $CD4^+$ T-cells, where STAT1 activity shapes the transcriptional output of STAT3 (12, 13). However, it is also noticeable that in the absence of IL-6, IFNγ-secreting Th1 cells promote enhanced STAT1 binding to these same loci. Thus, the altered balance of STAT1 and STAT3 binding to *Alu* sequences in *Il6* deficiency suggests that genes affiliated with these elements may be prone to cross-regulation.

The association of STAT transcription factors with *Alu* sequences affiliated with genes affecting tissue remodeling and fibrosis implies that these elements may promote disease progression. This conclusion comes with the proviso that functional interpretations of Alu binding are often challenging due to the complexities of mapping repetitive DNA elements. However, the increased number of peaks mapped to these motifs implies a link between *Alu*-like sequences and fibrosis or a propensity towards fibrosis. Genome-wide association studies recently identified human *Alu* polymorphisms linked with diseases described as interferonopathies or characterized by altered STAT1 activities (77-80). Our analysis of human GWAS datasets identified several targets common to mice treated with SES and Th1 cells. These data support a role for epigenetic modifiers that regulate the accessibility of transcription factors to specific enhancers under certain inflammatory

settings. Future evaluation of these events will open new opportunities to understand how cytokine cues are interpreted or become fine-tuned to direct physiology or pathophysiology.

Acknowledgements –

This manuscript is dedicated to Dr Javier Uceda Fernandez, a dearly loved friend and colleague who was tragically taken from us on the 29th of August 2018. Kidney Research UK (Reference RP-024-20160304 awarded to SAJ, DF, NT, GWJ), Versus Arthritis (Reference 20770, 19796, 20305 awarded to SAJ, VOD, NMW & GWJ), and the National Health and Medical Research Council of Australia (to BJJ) provided grant support for this project. JUF was recipient of a la Caixa PhD Studentship administered through the British Council, and BCC is supported by a PhD studentship from the Systems Immunity University Research Institute at Cardiff. JL is recipient of a Rutherford Fellowship Grant. PRT is recipient of a Wellcome Trust Investigator Award (Reference 107964/Z/15/Z) and receives funding through the UK Dementia Research Institute. Bioinformatic analysis was developed with support from the Systems Immunity University Research Institute in Cardiff.

Materials and methods–

Animals– All procedures were performed under UK Home Office project license P05D6A456. Inbred wild type C57BL/6 male mice were purchased from Charles River UK. IL-6-deficient ($Il6^{-/-}$) (60) were bred under approved UK Home Office guidelines in Cardiff University. The $gp130^{Y757F:Y757F}$ and $gp130^{Y757F:Y757F}$:$Stat3^{+/-}$ mice have been previously described (36). Experiments were approved by the Animal Ethics Committee and included genetically matched $gp130^{+/+}$ littermate controls. All experiments were performed using age-matched 8-12 weeks old mice.

SES-Induced Peritoneal Inflammation– A lyophilized cell-free supernatant prepared from *Staphylococcus epidermidis* (SES), whose activity had been standardized using an *in vitro* cell-based CXCL8 bioassay, was used to induce acute peritoneal inflammation (33). Mice were administered (i.p.) with a defined dose of SES (500µl). Soluble gp130Fc was added (i.p.) to WT mice as indicated. At 3 and 6 hours post-inflammatory challenge, mice were sacrificed and the peritoneal cavity lavaged with 2ml ice cold PBS. The peritoneal membrane was harvested at the same time points.

Transfer of Th1 Cells– To replicate events promoting peritoneal fibrosis some mice receiving SES were also simultaneously administered with either naïve $CD4^+$ T-cells or $CD4^+$ T-cells conditioned *ex vivo* towards a Th1 phenotype. Briefly, splenic naïve $CD4^+$ T-cells ($CD4^+CD25^-CD44^{lo}CD62L^{hi}$) were flow sorted and place in coated plates with anti-CD3e (145-2C11) and 5µg/ml soluble anti-CD28 (37.51) antibodies. Cells were cultured for 4 days in the presence of 20ng/ml murine recombinant IL-12 (R&D systems; 419-ML). The proportion of IFNγ-secreting $CD4^+$ T-cells (Th1 cells) was determined by intracellular flow cytometry using antibodies against to CD4 (RM4-5), IFNγ (XMG1.2), IL-17 (TC11-18H10.1), IL-4 (11B11) and IL-13 (eBio13A). Based on this analysis, T-cells were washed in ice cold PBS, re-suspended in a 500µl aliquot of PBS reconstituted SES, and administered via the intraperitoneal route. Here, a cell concentration of 5-10 $x10^5$ $CD4^+$ T-cells was administered to reflect the proportion of Th1 cells recruited to the peritoneal cavity under acute SES challenge. Where indicated, control mice were administered the same number of sorted naïve (Th0) $CD4^+$ T-cells. Changes in the inflammatory infiltrate were analyzed by direct counting (Coulter Z2, Beckman Coulter), differential cell counting and flow cytometry approaches using antibodies against defined leukocyte subsets. The peritoneal membrane was harvested at 3 and 6h after the injections.

Fluorescent labelling of bacteria– An inoculum of *Staphylococcus epidermidis* ATCC 12228 ($5x10^8$ cfu/mouse) was prepared from log phase cultures under sterile conditions. The suspension was centrifuged, and bacteria labelled for 20 min at 37°C in pre-warmed PBS containing Cell Trace Far Red (CT-FR) (Life Technologies) (1 µM or 8 µM for *ex vivo* and *in vivo* experiments, respectively). For *ex vivo* experiments, bacteria were serum-opsonized while, for *in vivo* experiments were centrifuged and washed 3 times in PBS, before resuspending in sterile PBS.

Ex vivo neutrophil effector function assay– Whole blood was collected by cardiac puncture into tubes containing 5mM EDTA. Samples were diluted 1:10 and washed 3 times in ice cold PBS. Cells were resuspended in serum-free RPMI 1640 containing 5 µM of 3'-(p-aminophenyl) fluorescein (APF) and incubated for 30 min at 37°C. APF-loaded cells were split into 100 µl aliquots and cultured at 37°C with an equal volume of pre-warmed, opsonized Cell Trace Far Red (CT-FR; 1 µM) labelled *S. epidermidis*. Cells were incubated for set time intervals (0-30 min) and transferred to an iced water bath prior to preparation for flow cytometry using a Beckman Coulter Cyan-ADP flow cytometer.

In vivo neutrophil effector function assay– Mice were administered (i.p.) with Cell Trace Far Red (CT-FR; 8 µM) labelled *S. epidermidis*. An independent group of *Il6*$^{-/-}$ mice received a dose of CT-FR labelled *S. epidermidis* together with the IL-6-sIL-6R chimeric fusion protein HDS (50 ng/ml). Six hours after bacterial challenge, the peritoneal cavity was lavaged with 2 ml of RPMI 1640 containing 5 µM of 3'-(p-aminophenyl) fluorescein (APF). Neutrophil phagocytosis and respiratory burst activity were examined by flow cytometry using a Beckman Coulter Cyan-ADP flow cytometer and analyzed using *Summit* (software v4.3, Beckman-Coulter) or FlowJo 10 (TreeStar).

Imaging flow cytometry analysis– Lavaged neutrophils were immune-stained for Ly6G (1A8), cells were resuspended in 100 µl of sterile PBS, and events (>8000 events per sample) were acquired at a low imaging rate and 60X amplification using the Amnis ImageStream®X Mark II Imaging Flow Cytometer (Amnis). Neutrophils were gated according to Ly6G staining. Phagocytic activity was expressed as a Phagocytic Index, which reflects the number of bacteria ingested by an individual Ly6G$^+$ neutrophil during the incubation period. To evaluate the phagocytic index of neutrophils undergoing phagocytosis, the Application "Spot Counting" in ImageStream software IDEAS (Amnis) was used. Spots were counted based on the distribution of CT-FR bacterial staining. The efficiency

of phagocytic uptake was quantified by examining cells displaying either a low (1-2 counts) or a high number (3 counts or more) of ingested bacteria.

Immunoblotting of peritoneal tissues– Protein was extracted from frozen peritoneal biopsies using ice-cold lysis buffer. Samples were pre-cleared of cellular debris before separation by SDS-PAGE and immunoblotting with specific antibodies against STAT1, STAT3 and tyrosine phosphorylated forms of STAT1 (pY-STAT1) and STAT3 (pY-STAT3) (36). Immuno-labelled proteins were detected using either the enhanced chemiluminescence (ECL) detection system (Amersham Biosciences) or Odyssey Infrared Imaging System (LI-COR, Lincoln, New England) with the appropriate secondary antibodies as per the manufacturer's instructions.

RNA-seq– Peritoneal membrane sections (80mg tissue) were dissociated in 1ml buffer RLT (QIAGEN) supplemented with β-mercaptoethanol (1:100 v:v) using a handheld electric homogeniser (Benchmark Scientific). Lysate was diluted 1:3 in distilled water and digested in 0.2mg/ml proteinase-K (Invitrogen; 25530049) for 10 minutes at 55°C. Lysate was cleared and RNA precipitated in 70% ethanol. Total RNA was extracted using the RNeasy Mini kit (QIAGEN) following the manufacturer's instructions. 2-4mg of mRNA was processed to generate the libraries. Cytoplasmic, mitochondrial, and ribosomal RNA was depleted using the Ribominus transcriptome isolation kit (Ambion; K155001). Libraries were prepared using the RNA-seq kit v2 (Life technologies; 4475936) and sequencing on an ion torrent (Thermo Fisher).

Chromatin Immunoprecipitation (ChIP)-seq– Excised peritoneal membranes were immediately frozen in liquid nitrogen and stored at -80°C until use. Tissues were diced and ground to a fine powder with intermittent addition of liquid nitrogen. Genomic DNA was extracted, crosslinked, and fragmented by sonication prior to treatment with 2µg/ml of anti-STAT1 (sc-592, Santa Cruz Biotechnology), anti-STAT3 (sc-482, Santa Cruz Biotechnology), anti-P300 (05-257, Millipore), or isotype control antibodies. Immunoprecipitation was conducted overnight at 4°C under continuous gentle agitation. Antigen-antibody complexes were captured using Protein-A/G magnetic beads, washed and DNA fragments liberated following treatment with proteinase-K and extraction with phenol-chloroform. Biological repeats from 3 independent tissue extracts were pooled and concentrated before the library preparation and next generation sequencing. ChIP libraries were prepared according to the manufacturer's instructions (Illumina Truseq DNA ChIP kit; RS-122-2001).

Size selection (200-400bp) was determined using a Blue Pippin (Sage Science) system employing 2% agarose cartridges (Sage Science; BDF2003). Appropriate library size distribution was confirmed using an Agilent 2100 bioanalyser and final concentrations determined using Qubit (Invitrogen). Libraries were sequenced on an Illumina HiSeq4000.

ATAC-seq– Excised peritoneal membranes were immediately frozen in liquid nitrogen and stored at -80°C until use. Tissues were diced and ground to a fine powder with intermittent addition of liquid nitrogen. Omni-ATAC seq was performed as described previously (81). Briefly, 100,000 nuclei per sample were isolated using an iodixanol gradient and ATAC-seq was subsequently performed according to the original protocol (82) using Nextera DNA Sample preparation kit (Illumina, FC-121-1030). After library amplification, DNA was isolated using Qiagen MiniElute kit and size selection was performed using Blue Pippin (Sage Science) system employing 2% agarose cartridges (Sage Science; BDF2003). Libraries were sequenced on an Illumina HiSeq4000.

Quantification and Statistical Analysis– No randomization and no blinding were used for the animal experiments. Whenever possible, the investigator was partially blinded for assessing the outcome. All data were analyzed using Prism 8 (GraphPad Prism, La Jolla, CA). Information on the types of Statistical methods used, the sample size and number of repetitions are listed in the Legends.

RNA-seq data analysis– Raw fastq were mapped using Torrent SuiteTM to the *mm10* reference genome and counts were assigned to transcripts using featureCounts (83) with the GRCm38.84 Ensembl gene build GTF. Differential gene expression analyses used the DESeq2 package (84). Genes were discarded from the analysis differential expression failed to be significant (significance: adj.pval < 0.05, Benjamini-Hochberg correction for multiple testing). Differentially regulated genes were uploaded into Ingenuity Pathway Analysis (IPA) (QIAGEN) for functional analysis.

ChIP-seq data analysis– Between 40-70M reads were obtained for each sample. These were trimmed with Trim Galore (https://www.bioinformatics.babraham.ac.uk/projects/trim_galore/) and assessed for quality using FastQC (https://www.bioinformatics.babraham.ac.uk/projects/fastqc/). Reads were mapped to the mouse mm10 reference genome using bwa (85). Peaks were called using macs2 (86), using the BAMPE model (adj.pval 0.05).

ATAC-seq analysis– Paired-end reads were processed with Trim Galore (https://www.bioinformatics.babraham.ac.uk/projects/trim_galore/) and assessed for quality using FastQC (https://www.bioinformatics.babraham.ac.uk/projects/fastqc/) prior to mapping to the mouse *mm10* reference genome (85). Peaks were called using macs2 and the BAMPE model (adj.pval 0.05)(86). Differential open-region analysis used Diffbind in Bioconductor (http://bioconductor.org/packages/release/bioc/vignettes/DiffBind/inst/doc/DiffBind.pdf). Histograms depicting distance from TSS were generated using the ChIPseeker R-package and show the peak count fraction.

Fantom5 enhancer analysis– Sequences annotated as enhancers by the Fantom5 consortium were downloaded from Slidebase (250bp pad) (http://slidebase.binf.ku.dk). Motif occurrences (n=8423, p<0.00001) in these sequences were identified using the FIMO algorithm (Meme ChIP-suite; http://meme-suite.org/tools/fimo). Genes in proximity to the identified sequences (defined as 2kb upstream or downstream) were mapped to the ensembl GRCh38 (hg38) build and visualized using the ClueGO cytoscape pluggin). Genome-wide motif occurrences were visualized with RIdeogram R-package (https://cran.r-project.org/web/packages/RIdeogram/vignettes/RIdeogram.html).

Motif identification– Sequences under ChIP peaks (q<0.05) were obtained using the bedtools getfasta command against the ensemble *mm10* genome build. Sequence fasta files were uploaded to Meme ChIP (http://meme-suite.org/tools/meme-chip) and searched against the murine HOCOMOCO (v11 CORE) and Eukaryote DNA databases. The *de novo* GAS-like motif was enriched by both Centrimo and Meme algorithms.

Spaced motif analysis– Analysis was conducted with Spamo (Meme-ChIP-suite) using default parameters. Secondary motifs occur within 150bp of the user-provided primary motif (GAS-like). All secondary motifs are referenced in the HOCOMOCO (v11 CORE) database. Input sequences, including a 250bp pad, were derived from the ChIP-seq data or enhancer annotations in Fantom5.

Multiple Sequence Alignment– Consensus sequences (Hidden Markov Models) corresponding to murine and human Alu-family transposable elements were downloaded from the Dfam database (https://dfam.org/) - Mouse; B1_mm, B1_mus1, PB1D11, B1_Mur2, B1_Mur4, PB1, B1_Mur1, B1_Mur3, PB1D10, B1_Mus2, B1_F1, PB1D7, PB1D9, B1F2, B1F, B2_Mm1a, B2_Mm1t, B2_Mm2, B3, B3A, B4, B4A, ID_B1, Human; AluY, AluSc, AluJB, AluJo, AluJr, AluJr4, AluSc5, AluSc8, AluSg,

AluSg4, AluSg7, AluSp, AluSq, AluSq10, AluSq2, AluSq4, AluSx, AluSx1, AluSx3, AluSx4, AluSz, AluSz6, AluYa5, AluYa8, AluYb8, AluYb9, AluYc, AluYc3, AluYd8, AluYh9, AluYk11, AluYk12, AluYk4, AluYg6, AluYk3, AluYm1, AluYk2, AluYe6, AluYi6, AluYe5, AluYi6_4d, AluYf1, AluYh3, AluYj4, AluYh7, FAM, FLAMA, FLAMC, FRAM. Sequences were aligned using MUSCLE (European Bioinformatics Institute) using the default ClustalW output and visualized in Jalview.

Gene Set Enrichment Analysis (GSEA)– A ranked gene list was prepared for each dataset using the differential gene expression analysis. Using the GSEA pre-ranked function, enrichment profiles were generated against the biological processes (C-5; 7573 gene sets) gene ontology database. For visualization, GSEA output files were loaded into Cytoscape using the enrichment-map plugin. For small gene sets, ontology enrichments were performed using either the mSigdb overlap tool (broad institute) or the Metascape online tool. Network aesthetics (e.g., color, spacing) were modified in adobe illustrator. Network statistical thresholds are below $p<0.01$, $q<0.01$.

Repeatmasker overlaps– Alu and L1 sequence coordinates were derived from the repeatmasker definitions downloaded from the UCSC table browser (*mm10*). Repeats overlapping STAT binding were identified using the bedtools intersect algorithm. The absolute number of Alu and L1 sequences overlapping each ChIP dataset was calculated in R studio and plotted using the circlize package.

Network analysis of gene expression clustering– The differential gene expression analysis for a subset of K-means clustered genes was correlated and converted to an adjacency matrix in R studio. Data were hierarchically clustered (Euclidean) and converted to a network in the R package igraph. Colors were selected form the R Color Brewer package. Network edges have been hidden to aid visualization. Node size is proportional to Degree, with each node representing a gene that is either up or downregulated in the differential gene expression analysis.

Visualization and annotation– Heatmap visualization in Morpheus (broad institute) and Pheatmap (R package) using colours defined in the viridis and R Color Brewer packages. Figures were prepared using the ggplot2 R package (R package), graphpad prism8, and arranged in Adobe Illustrator. Data filtering for complex heatmaps was achieved using Dplyr (R package). IL-6 regulated genes were defined as those meeting the statistical threshold (*Il6*$^{-/-}$ vs wt padj<0.05) in at least one

experimental condition. STAT regulated genes were similarly described as those with ChIP signal under the statistical threshold (q<0.05) in at least one experimental condition.

Generation of gene sets for Magma analysis– Sequences annotated as enhancers by the Fantom5 consortium were downloaded from Slidebase (http://slidebase.binf.ku.dk/) including a 200bp pad. To identify motif occurrences, these sequences were entered to the FIMO web server (Meme ChIP suite) together with the MEME-formatted motif extracted from our ChIP-sequencing analyses. Identified gene sets were derived by mapping coordinates to the HG19 reference genome (genes within 2kb) using PAVIS (https://manticore.niehs.nih.gov/pavis2/). In parallel, Fantom5 sequences containing Alu sequences were defined by intersecting (bedtools) Fantom5 coordinates with the Repeatmasker database (UCSC table browser). Coordinates were mapped to genes using PAVIS. Randomised control gene sets were derived as follows. (1) FIMO output coordinates were 'shuffled' across Fantom sequences or genome wide (Hg19 reference genome) using the Bedtools shuffle feature. (2) Random bed files (8000x 500bp sequences) were generated using the Bedtools Random against either the Fantom5 enhancer sequences or genome wide (hg19). Three gene sets were generated for each control. Hallmark gene sets were downloaded from msigdb (broad Institute). Genes mapping to the MHC locus were downloaded from the UCSC table browser. This gene list was used to filter MHC-locus genes from all gene sets prior to Magma analysis (Dplyr R-package).

Magma– GWAS summary statistics (Hg19) were downloaded using FTP links supplied by the GWAS atlas (https://atlas.ctglab.nl/). After re-formatting for compatibility with magma, summary statistics were mapped to genes using the build-37 gene locations file (NCBI37.3.gene.loc). Gene results files were next generated for each summary statistic. The GWAS atlas was used to refence N (number of study participants) for each study. Finally, gene set analysis was performed against gene sets generated as described above. Results files were read into R and relevant columns extracted using R base functions. For genes, p-values were extracted from magma output files ending genes.sets.out. For gene sets, p-values were extracted from output files ending.gsa.out. P-values were merged into a single dataframe for correlation analysis (R-base function) or filtering (Dplyr R-package). Heatmaps were generated using the Pretty heatmap R package (Pheatmap).

Data and Code Availability– RNA-seq, ChIP-seq and ATAC-seq datasets reported in this paper have been deposited in ArrayExpress under accession code EMBL-EBIE-MTAB-10087. The authors declare

that all relevant data supporting the findings of this study are available on request. R scripts for performing the main steps of analysis are available from the Lead contact on reasonable request.

References–

1. Dinarello, C. 2007. Historical insights into cytokines. *Eur J Immunol* 37: S34-45.

2. Choy, E. H., A. F. Kavanaugh, and S. A. Jones. 2013. The problem of choice: current biologic agents and future prospects in RA. *Nat Rev Rheumatol* 9: 154-163.

3. Hunter, C. A., and S. A. Jones. 2015. IL-6 as a keystone cytokine in health and disease. *Nat Immunol* 16: 448-457.

4. Schett, G., D. Elewaut, I. B. McInnes, J. M. Dayer, and M. F. Neurath. 2013. How cytokine networks fuel inflammation: Toward a cytokine-based disease taxonomy. *Nature medicine* 19: 822-824.

5. Jones, S. A., J. Scheller, and S. Rose-John. 2011. Therapeutic strategies for the clinical blockade of IL-6/gp130 signaling. *The Journal of clinical investigation* 121: 3375-3383.

6. Jones, S. A., and B. J. Jenkins. 2018. Recent insights into targeting the IL-6 cytokine family in inflammatory diseases and cancer. *Nat Rev Immunol* 18: 773-789.

7. Taniguchi, K., L. W. Wu, S. I. Grivennikov, P. R. de Jong, I. Lian, F. X. Yu, K. Wang, S. B. Ho, B. S. Boland, J. T. Chang, W. J. Sandborn, G. Hardiman, E. Raz, Y. Maehara, A. Yoshimura, J. Zucman-Rossi, K. L. Guan, and M. Karin. 2015. A gp130-Src-YAP module links inflammation to epithelial regeneration. *Nature* 519: 57-62.

8. Andrews, C., M. H. McLean, and S. K. Durum. 2018. Cytokine Tuning of Intestinal Epithelial Function. *Front Immunol* 9: 1270.

9. Harbour, S. N., D. F. DiToro, S. J. Witte, C. L. Zindl, M. Gao, T. R. Schoeb, G. W. Jones, S. A. Jones, R. D. Hatton, and C. T. Weaver. 2020. TH17 cells require ongoing classic IL-6 receptor signaling to retain transcriptional and functional identity. *Sci Immunol* 5.

10. Navarini, A. A., L. E. French, and G. F. Hofbauer. 2011. Interrupting IL-6-receptor signaling improves atopic dermatitis but associates with bacterial superinfection. *The Journal of allergy and clinical immunology* 128: 1128-1130.

11. Villarino, A. V., Y. Kanno, and J. J. O'Shea. 2017. Mechanisms and consequences of Jak-STAT signaling in the immune system. *Nat Immunol* 18: 374-384.

12. Hirahara, K., A. Onodera, A. V. Villarino, M. Bonelli, G. Sciume, A. Laurence, H. W. Sun, S. R. Brooks, G. Vahedi, H. Y. Shih, G. Gutierrez-Cruz, S. Iwata, R. Suzuki, Y. Mikami, Y. Okamoto, T. Nakayama, S. M. Holland, C. A. Hunter, Y. Kanno, and J. J. O'Shea. 2015. Asymmetric Action of STAT Transcription Factors Drives Transcriptional Outputs and Cytokine Specificity. *Immunity* 42: 877-889.

13. Peters, A., K. D. Fowler, F. Chalmin, D. Merkler, V. K. Kuchroo, and C. Pot. 2015. IL-27 Induces Th17 Differentiation in the Absence of STAT1 Signaling. *J Immunol* 195: 4144-4153.

14. Jones, G. W., C. J. Greenhill, J. O. Williams, M. A. Nowell, A. S. Williams, B. J. Jenkins, and S. A. Jones. 2013. Exacerbated inflammatory arthritis in response to hyperactive gp130 signalling is independent of IL-17A. *Ann Rheum Dis* 72: 1738-1742.

15. Costa-Pereira, A. P., S. Tininini, B. Strobl, T. Alonzi, J. F. Schlaak, H. Is'harc, I. Gesualdo, S. J. Newman, I. M. Kerr, and V. Poli. 2002. Mutational switch of an IL-6 response to an interferon-gamma-like response. *Proc Natl Acad Sci U S A* 99: 8043-8047.

16. Twohig, J., Cardus Figueras, A., Andrews, R., Wiede, F., Cossins, BC., Derrac Soria, A., Lewis, M., Townsend, MJ., Millrine, D., Li, J., Hill, D., Uceda Fernandez, J., Liu, X., Szomolay, B., Pepper, CJ., Taylor, PR., Pitzalis, C., Tiganis, T. Williams, NM., Jones, GW. & Jones, SA. 2019. Naïve T-cell activation re-tunes STAT1 signaling to deliver unique cytokine responses in memory CD4 T-cells. *Nature Immunology* 20: 458-470.

17. Wilmes, S., P. A. Jeffrey, J. Martinez-Fabregas, M. Hafer, P. K. Fyfe, E. Pohler, S. Gaggero, M. Lopez-Garcia, G. Lythe, C. Taylor, T. Guerrier, D. Launay, S. Mitra, J. Piehler, C. Molina-Paris, and I. Moraga. 2021. Competitive binding of STATs to receptor phospho-Tyr motifs accounts for altered cytokine responses. *Elife* 10.

18. Vahedi, G., Y. Kanno, Y. Furumoto, K. Jiang, S. C. Parker, M. R. Erdos, S. R. Davis, R. Roychoudhuri, N. P. Restifo, M. Gadina, Z. Tang, Y. Ruan, F. S. Collins, V. Sartorelli, and J. J. O'Shea. 2015. Super-enhancers delineate disease-associated regulatory nodes in T cells. *Nature* 520: 558-562.

19. Avalle, L., S. Pensa, G. Regis, F. Novelli, and V. Poli. 2012. STAT1 and STAT3 in tumorigenesis: A matter of balance. *JAKSTAT* 1: 65-72.

20. Jones, G. W., M. Bombardieri, C. J. Greenhill, L. McLeod, A. Nerviani, V. Rocher-Ros, A. Cardus, A. S. Williams, C. Pitzalis, B. J. Jenkins, and S. A. Jones. 2015. Interleukin-27 inhibits ectopic lymphoid-like structure development in early inflammatory arthritis. *J Exp Med* 212: 1793-1802.

21. Fielding, C. A., G. W. Jones, R. M. McLoughlin, L. McLeod, V. J. Hammond, J. Uceda, A. S. Williams, M. Lambie, T. L. Foster, C. T. Liao, C. M. Rice, C. J. Greenhill, C. S. Colmont, E. Hams, B. Coles, A. Kift-Morgan, Z. Newton, K. J. Craig, J. D. Williams, G. T. Williams, S. J. Davies, I. R. Humphreys, V. B. O'Donnell, P. R. Taylor, B. J. Jenkins, N. Topley, and S. A. Jones. 2014. Interleukin-6 signaling drives fibrosis in unresolved inflammation. *Immunity* 40: 40-50.

22. Hong, F., B. Jaruga, W. H. Kim, S. Radaeva, O. N. El-Assal, Z. Tian, V. A. Nguyen, and B. Gao. 2002. Opposing roles of STAT1 and STAT3 in T cell-mediated hepatitis: regulation by SOCS. *The Journal of clinical investigation* 110: 1503-1513.

23. Wiede, F., T. C. Brodnicki, P. K. Goh, Y. A. Leong, G. W. Jones, D. Yu, A. G. Baxter, S. A. Jones, T. W. H. Kay, and T. Tiganis. 2019. T-Cell-Specific PTPN2 Deficiency in NOD Mice Accelerates the Development of Type 1 Diabetes and Autoimmune Comorbidities. *Diabetes* 68: 1251-1266.

24. Grohmann, M., F. Wiede, G. T. Dodd, E. N. Gurzov, G. J. Ooi, T. Butt, A. A. Rasmiena, S. Kaur, T. Gulati, P. K. Goh, A. E. Treloar, S. Archer, W. A. Brown, M. Muller, M. J. Watt, O. Ohara, C. A. McLean, and T. Tiganis. 2018. Obesity Drives STAT-1-Dependent NASH and STAT-3-Dependent HCC. *Cell* 175: 1289-1306 e1220.

25. Lin, J. X., and W. J. Leonard. 2019. Fine-Tuning Cytokine Signals. *Annu Rev Immunol* 37: 295-324.

26. Martinez-Fabregas, J., L. Wang, E. Pohler, A. Cozzani, S. Wilmes, M. Kazemian, S. Mitra, and I. Moraga. 2020. CDK8 Fine-Tunes IL-6 Transcriptional Activities by Limiting STAT3 Resident Time at the Gene Loci. *Cell Rep* 33: 108545.

27. Krausgruber, T., N. Fortelny, V. Fife-Gernedl, M. Senekowitsch, L. C. Schuster, A. Lercher, A. Nemc, C. Schmidl, A. F. Rendeiro, A. Bergthaler, and C. Bock. 2020. Structural cells are key regulators of organ-specific immune responses. *Nature* 583: 296-302.

28. Gomes, T., and S. A. Teichmann. 2020. An antiviral response beyond immune cells. *Nature* 583: 206-207.

29. Jones, S. A. 2005. Directing transition from innate to acquired immunity: defining a role for IL-6. *J Immunol* 175: 3463-3468.

30. Cho, Y., D. W. Johnson, D. A. Vesey, C. M. Hawley, E. M. Pascoe, M. Clarke, N. Topley, and A. N. Z. T. I. bal. 2014. Dialysate interleukin-6 predicts increasing peritoneal solute transport rate in incident peritoneal dialysis patients. *BMC Nephrol* 15: 8.

31. Catar, R., J. Witowski, N. Zhu, C. Lucht, A. Derrac Soria, J. Uceda Fernandez, L. Chen, S. A. Jones, C. A. Fielding, A. Rudolf, N. Topley, D. Dragun, and A. Jorres. 2017. IL-6 Trans-Signaling Links Inflammation with Angiogenesis in the Peritoneal Membrane. *J Am Soc Nephrol* 28: 1188-1199.

32. Jones, G. W., R. M. McLoughlin, V. J. Hammond, C. R. Parker, J. D. Williams, R. Malhotra, J. Scheller, A. S. Williams, S. Rose-John, N. Topley, and S. A. Jones. 2010. Loss of CD4+ T cell IL-6R expression during inflammation underlines a role for IL-6 trans signaling in the local maintenance of Th17 cells. *J Immunol* 184: 2130-2139.

33. Hurst, S. M., T. S. Wilkinson, R. M. McLoughlin, S. Jones, S. Horiuchi, N. Yamamoto, S. Rose-John, G. M. Fuller, N. Topley, and S. A. Jones. 2001. Il-6 and its soluble receptor orchestrate a temporal switch in the pattern of leukocyte recruitment seen during acute inflammation. *Immunity* 14: 705-714.

34. McLoughlin, R. M., S. M. Hurst, M. A. Nowell, D. A. Harris, S. Horiuchi, L. W. Morgan, T. S. Wilkinson, N. Yamamoto, N. Topley, and S. A. Jones. 2004. Differential regulation of neutrophil-activating chemokines by IL-6 and its soluble receptor isoforms. *J Immunol* 172: 5676-5683.

35. McLoughlin, R. M., B. J. Jenkins, D. Grail, A. S. Williams, C. A. Fielding, C. R. Parker, M. Ernst, N. Topley, and S. A. Jones. 2005. IL-6 trans-signaling via STAT3 directs T cell infiltration in acute inflammation. *Proc Natl Acad Sci U S A* 102: 9589-9594.

36. Jenkins, B. J., D. Grail, T. Nheu, M. Najdovska, B. Wang, P. Waring, M. Inglese, R. M. McLoughlin, S. A. Jones, N. Topley, H. Baumann, L. M. Judd, A. S. Giraud, A. Boussioutas, H. J. Zhu, and M. Ernst. 2005. Hyperactivation of Stat3 in gp130 mutant mice promotes gastric hyperproliferation and desensitizes TGF-beta signaling. *Nature medicine* 11: 845-852.

37. Fielding, C. A., R. M. McLoughlin, L. McLeod, C. S. Colmont, M. Najdovska, D. Grail, M. Ernst, S. A. Jones, N. Topley, and B. J. Jenkins. 2008. IL-6 regulates neutrophil trafficking during acute inflammation via STAT3. *J Immunol* 181: 2189-2195.

38. McLoughlin, R. M., J. Witowski, R. L. Robson, T. S. Wilkinson, S. M. Hurst, A. S. Williams, J. D. Williams, S. Rose-John, S. A. Jones, and N. Topley. 2003. Interplay between IFN-gamma and IL-6 signaling governs neutrophil trafficking and apoptosis during acute inflammation. *The Journal of clinical investigation* 112: 598-607.

39. Robson, R. L., R. M. McLoughlin, J. Witowski, P. Loetscher, T. S. Wilkinson, S. A. Jones, and N. Topley. 2001. Differential regulation of chemokine production in human peritoneal mesothelial cells: IFN-gamma controls neutrophil migration across the mesothelium in vitro and in vivo. *J Immunol* 167: 1028-1038.

40. Vahedi, G., H. Takahashi, S. Nakayamada, H. W. Sun, V. Sartorelli, Y. Kanno, and J. J. O'Shea. 2012. STATs shape the active enhancer landscape of T cell populations. *Cell* 151: 981-993.

41. Hutchins, A. P., D. Diez, and D. Miranda-Saavedra. 2013. Genomic and computational approaches to dissect the mechanisms of STAT3's universal and cell type-specific functions. *JAKSTAT* 2: e25097.

42. Ferrari, R., L. I. de Llobet Cucalon, C. Di Vona, F. Le Dilly, E. Vidal, A. Lioutas, J. Q. Oliete, L. Jochem, E. Cutts, G. Dieci, A. Vannini, M. Teichmann, S. de la Luna, and M. Beato. 2020. TFIIIC Binding to Alu Elements Controls Gene Expression via Chromatin Looping and Histone Acetylation. *Mol Cell* 77: 475-487.e411.

43. Duffield, J. S., M. Lupher, V. J. Thannickal, and T. A. Wynn. 2013. Host responses in tissue repair and fibrosis. *Annu Rev Pathol* 8: 241-276.

44. Borthwick, L. A., T. A. Wynn, and A. J. Fisher. 2013. Cytokine mediated tissue fibrosis. *Biochim Biophys Acta* 1832: 1049-1060.

45. Yang, X., H. Yan, N. Jiang, Z. Yu, J. Yuan, Z. Ni, and W. Fang. 2020. IL-6 trans-signaling drives a STAT3-dependent pathway that leads to structural alterations of the peritoneal membrane. *Am J Physiol Renal Physiol* 318: F338-F353.

46. Modur, V., Y. Li, G. A. Zimmerman, S. M. Prescott, and T. M. McIntyre. 1997. Retrograde inflammatory signaling from neutrophils to endothelial cells by soluble interleukin-6 receptor alpha. *The Journal of clinical investigation* 100: 2752-2756.

47. Xing, Z., J. Gauldie, G. Cox, H. Baumann, M. Jordana, X. F. Lei, and M. K. Achong. 1998. IL-6 is an antiinflammatory cytokine required for controlling local or systemic acute inflammatory responses. *The Journal of clinical investigation* 101: 311-320.

48. Qing, Y., and G. R. Stark. 2004. Alternative activation of STAT1 and STAT3 in response to interferon-gamma. *J Biol Chem* 279: 41679-41685.

49. Yang, X. P., K. Ghoreschi, S. M. Steward-Tharp, J. Rodriguez-Canales, J. Zhu, J. R. Grainger, K. Hirahara, H. W. Sun, L. Wei, G. Vahedi, Y. Kanno, J. J. O'Shea, and A. Laurence. 2011. Opposing regulation of the locus encoding IL-17 through direct, reciprocal actions of STAT3 and STAT5. *Nat Immunol* 12: 247-254.

50. Ernst, M., M. Najdovska, D. Grail, T. Lundgren-May, M. Buchert, H. Tye, V. B. Matthews, J. Armes, P. S. Bhathal, N. R. Hughes, E. G. Marcusson, J. G. Karras, S. Na, J. D. Sedgwick, P. J. Hertzog, and B. J. Jenkins. 2008. STAT3 and STAT1 mediate IL-11-dependent and inflammation-associated gastric tumorigenesis in gp130 receptor mutant mice. *The Journal of clinical investigation* 118: 1727-1738.

51. Olbrich, P., and A. F. Freeman. 2018. STAT1 and STAT3 mutations: important lessons for clinical immunologists. *Expert Rev Clin Immunol* 14: 1029-1041.

52. Luis, B. A. L., and J. J. Calva-Mercado. 2018. Recurrent Spontaneous Intestinal Perforation due to STAT1 GOF Mutation. *Am J Gastroenterol* 113: 1057-1058.

53. Toubiana, J., S. Okada, J. Hiller, M. Oleastro, M. Lagos Gomez, J. C. Aldave Becerra, M. Ouachee-Chardin, F. Fouyssac, K. M. Girisha, A. Etzioni, J. Van Montfrans, Y. Camcioglu, L. A. Kerns, B. Belohradsky, S. Blanche, A. Bousfiha, C. Rodriguez-Gallego, I. Meyts, K. Kisand, J. Reichenbach, E. D. Renner, S. Rosenzweig, B. Grimbacher, F. L. van de Veerdonk, C. Traidl-Hoffmann, C. Picard, L. Marodi, T. Morio, M. Kobayashi, D. Lilic, J. D. Milner, S. Holland, J. L. Casanova, A. Puel, and S. G.-o.-F. S. G. International. 2016. Heterozygous STAT1 gain-of-function mutations underlie an unexpectedly broad clinical phenotype. *Blood* 127: 3154-3164.

54. Milner, J. D., T. P. Vogel, L. Forbes, C. A. Ma, A. Stray-Pedersen, J. E. Niemela, J. J. Lyons, K. R. Engelhardt, Y. Zhang, N. Topcagic, E. D. Roberson, H. Matthews, J. W. Verbsky, T. Dasu, A. Vargas-Hernandez, N. Varghese, K. L. McClain, L. B. Karam, K. Nahmod, G. Makedonas, E. M. Mace, H. S. Sorte, G. Perminow, V. K. Rao, M. P. O'Connell, S. Price, H. C. Su, M. Butrick, J. McElwee, J. D. Hughes, J. Willet, D. Swan, Y. Xu, M. Santibanez-Koref, V. Slowik, D. L. Dinwiddie, C. E. Ciaccio, C. J. Saunders, S. Septer, S. F. Kingsmore, A. J. White, A. J. Cant, S. Hambleton, and M. A. Cooper. 2015. Early-onset lymphoproliferation and autoimmunity caused by germline STAT3 gain-of-function mutations. *Blood* 125: 591-599.

55. Goel, S., S. Sahu, R. W. Minz, S. Singh, D. Suri, Y. M. Oh, A. Rawat, S. Sehgal, and B. Saikia. 2018. STAT3-Mediated Transcriptional Regulation of Osteopontin in STAT3 Loss-of-Function Related Hyper IgE Syndrome. *Front Immunol* 9: 1080.

56. Abusleme, L., P. I. Diaz, A. F. Freeman, T. Greenwell-Wild, L. Brenchley, J. V. Desai, W. I. Ng, S. M. Holland, M. S. Lionakis, J. A. Segre, H. H. Kong, and N. M. Moutsopoulos. 2018. Human defects in STAT3 promote oral mucosal fungal and bacterial dysbiosis. *JCI Insight* 3.

57. Liu, L., S. Okada, X. F. Kong, A. Y. Kreins, S. Cypowyj, A. Abhyankar, J. Toubiana, Y. Itan, M. Audry, P. Nitschke, C. Masson, B. Toth, J. Flatot, M. Migaud, M. Chrabieh, T. Kochetkov, A. Bolze, A. Borghesi, A. Toulon, J. Hiller, S. Eyerich, K. Eyerich, V. Gulacsy, L. Chernyshova, V. Chernyshov, A. Bondarenko, R. M. Grimaldo, L. Blancas-Galicia, I. M. Beas, J. Roesler, K. Magdorf, D. Engelhard, C. Thumerelle, P. R. Burgel, M. Hoernes, B. Drexel, R. Seger, T. Kusuma, A. F. Jansson, J. Sawalle-Belohradsky, B. Belohradsky, E. Jouanguy, J. Bustamante, M. Bue, N. Karin, G. Wildbaum, C. Bodemer, O. Lortholary, A. Fischer, S. Blanche, S. Al-Muhsen, J. Reichenbach, M. Kobayashi, F. E. Rosales, C. T. Lozano, S. S. Kilic, M. Oleastro, A. Etzioni, C. Traidl-Hoffmann, E. D. Renner, L. Abel, C. Picard, L. Marodi, S. Boisson-Dupuis, A. Puel, and J. L. Casanova. 2011. Gain-of-function human STAT1 mutations impair IL-17 immunity and underlie chronic mucocutaneous candidiasis. *J Exp Med* 208: 1635-1648.

58. Spencer, S., S. Kostel Bal, W. Egner, H. Lango Allen, S. I. Raza, C. A. Ma, M. Gurel, Y. Zhang, G. Sun, R. A. Sabroe, D. Greene, W. Rae, T. Shahin, K. Kania, R. C. Ardy, M. Thian, E. Staples, A. Pecchia-Bekkum, W. P. M. Worrall, J. Stephens, M. Brown, S. Tuna, M. York, F. Shackley, D. Kerrin, R. Sargur, A. Condliffe, H. N. Tipu, H. S. Kuehn, S. D. Rosenzweig, E. Turro, S. Tavare, A. J. Thrasher, D. I. Jodrell, K. G. C. Smith, K. Boztug, J. D. Milner, and J. E. D. Thaventhiran. 2019. Loss of the interleukin-6 receptor causes immunodeficiency, atopy, and abnormal inflammatory responses. *J Exp Med*.

59. Ramsay, A. J., A. J. Husband, I. A. Ramshaw, S. Bao, K. I. Matthaei, G. Koehler, and M. Kopf. 1994. The role of interleukin-6 in mucosal IgA antibody responses in vivo. *Science* 264: 561-563.

60. Kopf, M., H. Baumann, G. Freer, M. Freudenberg, M. Lamers, T. Kishimoto, R. Zinkernagel, H. Bluethmann, and G. Kohler. 1994. Impaired immune and acute-phase responses in interleukin-6-deficient mice. *Nature* 368: 339-342.

61. Welte, T., S. S. Zhang, T. Wang, Z. Zhang, D. G. Hesslein, Z. Yin, A. Kano, Y. Iwamoto, E. Li, J. E. Craft, A. L. Bothwell, E. Fikrig, P. A. Koni, R. A. Flavell, and X. Y. Fu. 2003. STAT3 deletion during hematopoiesis causes Crohn's disease-like pathogenesis and lethality: a critical role of STAT3 in innate immunity. *Proc Natl Acad Sci U S A* 100: 1879-1884.

62. Kano, A., M. J. Wolfgang, Q. Gao, J. Jacoby, G. X. Chai, W. Hansen, Y. Iwamoto, J. S. Pober, R. A. Flavell, and X. Y. Fu. 2003. Endothelial cells require STAT3 for protection against endotoxin-induced inflammation. *J Exp Med* 198: 1517-1525.

63. Matsukawa, A., K. Takeda, S. Kudo, T. Maeda, M. Kagayama, and S. Akira. 2003. Aberrant inflammation and lethality to septic peritonitis in mice lacking STAT3 in macrophages and neutrophils. *J Immunol* 171: 6198-6205.

64. Holland, S. M., F. R. DeLeo, H. Z. Elloumi, A. P. Hsu, G. Uzel, N. Brodsky, A. F. Freeman, A. Demidowich, J. Davis, M. L. Turner, V. L. Anderson, D. N. Darnell, P. A. Welch, D. B. Kuhns, D. M. Frucht, H. L. Malech, J. I. Gallin, S. D. Kobayashi, A. R. Whitney, J. M. Voyich, J. M. Musser, C. Woellner, A. A. Schaffer, J. M. Puck, and B. Grimbacher. 2007. STAT3 mutations in the hyper-IgE syndrome. *N Engl J Med* 357: 1608-1619.

65. Blow, M. J., D. J. McCulley, Z. Li, T. Zhang, J. A. Akiyama, A. Holt, I. Plajzer-Frick, M. Shoukry, C. Wright, F. Chen, V. Afzal, J. Bristow, B. Ren, B. L. Black, E. M. Rubin, A. Visel, and L. A. Pennacchio. 2010. ChIP-Seq identification of weakly conserved heart enhancers. *Nat Genet* 42: 806-810.

66. Visel, A., M. J. Blow, Z. Li, T. Zhang, J. A. Akiyama, A. Holt, I. Plajzer-Frick, M. Shoukry, C. Wright, F. Chen, V. Afzal, B. Ren, E. M. Rubin, and L. A. Pennacchio. 2009. ChIP-seq accurately predicts tissue-specific activity of enhancers. *Nature* 457: 854-858.

67. Ciofani, M., A. Madar, C. Galan, M. Sellars, K. Mace, F. Pauli, A. Agarwal, W. Huang, C. N. Parkhurst, M. Muratet, K. M. Newberry, S. Meadows, A. Greenfield, Y. Yang, P. Jain, F. K. Kirigin, C. Birchmeier, E. F. Wagner, K. M. Murphy, R. M. Myers, R. Bonneau, and D. R. Littman. 2012. A validated regulatory network for Th17 cell specification. *Cell* 151: 289-303.

68. Paulson, M., S. Pisharody, L. Pan, S. Guadagno, A. L. Mui, and D. E. Levy. 1999. Stat protein transactivation domains recruit p300/CBP through widely divergent sequences. *J Biol Chem* 274: 25343-25349.

69. Ostuni, R., V. Piccolo, I. Barozzi, S. Polletti, A. Termanini, S. Bonifacio, A. Curina, E. Prosperini, S. Ghisletti, and G. Natoli. 2013. Latent enhancers activated by stimulation in differentiated cells. *Cell* 152: 157-171.

70. Natoli, G., S. Ghisletti, and I. Barozzi. 2011. The genomic landscapes of inflammation. *Genes Dev* 25: 101-106.

71. Tong, A. J., X. Liu, B. J. Thomas, M. M. Lissner, M. R. Baker, M. D. Senagolage, A. L. Allred, G. D. Barish, and S. T. Smale. 2016. A Stringent Systems Approach Uncovers Gene-Specific Mechanisms Regulating Inflammation. *Cell* 165: 165-179.

72. Vassetzky, N. S., and D. A. Kramerov. 2013. SINEBase: a database and tool for SINE analysis. *Nucleic Acids Res* 41: D83-89.

73. Chen, L. L., and L. Yang. 2017. ALUternative Regulation for Gene Expression. *Trends Cell Biol* 27: 480-490.

74. Tajnik, M., A. Vigilante, S. Braun, H. Hanel, N. M. Luscombe, J. Ule, K. Zarnack, and J. Konig. 2015. Intergenic Alu exonisation facilitates the evolution of tissue-specific transcript ends. *Nucleic Acids Res* 43: 10492-10505.

75. Xie, H., M. Wang, F. Bonaldo Mde, C. Smith, V. Rajaram, S. Goldman, T. Tomita, and M. B. Soares. 2009. High-throughput sequence-based epigenomic analysis of Alu repeats in human cerebellum. *Nucleic Acids Res* 37: 4331-4340.

76. Polak, P., and E. Domany. 2006. Alu elements contain many binding sites for transcription factors and may play a role in regulation of developmental processes. *BMC Genomics* 7: 133.

77. Payer, L. M., J. P. Steranka, W. R. Yang, M. Kryatova, S. Medabalimi, D. Ardeljan, C. Liu, J. D. Boeke, D. Avramopoulos, and K. H. Burns. 2017. Structural variants caused by Alu insertions are associated with risks for many human diseases. *Proc Natl Acad Sci U S A* 114: E3984-E3992.

78. Volkman, H. E., and D. B. Stetson. 2014. The enemy within: endogenous retroelements and autoimmune disease. *Nat Immunol* 15: 415-422.

79. Hung, T., G. A. Pratt, B. Sundararaman, M. J. Townsend, C. Chaivorapol, T. Bhangale, R. R. Graham, W. Ortmann, L. A. Criswell, G. W. Yeo, and T. W. Behrens. 2015. The Ro60 autoantigen binds endogenous retroelements and regulates inflammatory gene expression. *Science* 350: 455-459.

80. Zeng, M., Z. Hu, X. Shi, X. Li, X. Zhan, X. D. Li, J. Wang, J. H. Choi, K. W. Wang, T. Purrington, M. Tang, M. Fina, R. J. DeBerardinis, E. M. Moresco, G. Pedersen, G. M. McInerney, G. B. Karlsson Hedestam, Z. J. Chen, and B. Beutler. 2014. MAVS, cGAS, and endogenous retroviruses in T-independent B cell responses. *Science* 346: 1486-1492.

81. Corces, M. R., A. E. Trevino, E. G. Hamilton, P. G. Greenside, N. A. Sinnott-Armstrong, S. Vesuna, A. T. Satpathy, A. J. Rubin, K. S. Montine, B. Wu, A. Kathiria, S. W. Cho, M. R. Mumbach, A. C. Carter, M. Kasowski, L. A. Orloff, V. I. Risca, A. Kundaje, P. A. Khavari, T. J. Montine, W. J. Greenleaf, and H. Y. Chang. 2017. An improved ATAC-seq protocol reduces background and enables interrogation of frozen tissues. *Nat Methods* 14: 959-962.

82. Buenrostro, J. D., P. G. Giresi, L. C. Zaba, H. Y. Chang, and W. J. Greenleaf. 2013. Transposition of native chromatin for fast and sensitive epigenomic profiling of open chromatin, DNA-binding proteins and nucleosome position. *Nat Methods* 10: 1213-1218.

83. Liao, Y., G. K. Smyth, and W. Shi. 2014. featureCounts: an efficient general purpose program for assigning sequence reads to genomic features. *Bioinformatics* 30: 923-930.

84. Love, M. I., W. Huber, and S. Anders. 2014. Moderated estimation of fold change and dispersion for RNA-seq data with DESeq2. *Genome Biol* 15: 550.

85. Li, H., and R. Durbin. 2009. Fast and accurate short read alignment with Burrows-Wheeler transform. *Bioinformatics* 25: 1754-1760.

86. Zhang, Y., T. Liu, C. A. Meyer, J. Eeckhoute, D. S. Johnson, B. E. Bernstein, C. Nusbaum, R. M. Myers, M. Brown, W. Li, and X. S. Liu. 2008. Model-based analysis of ChIP-Seq (MACS). *Genome Biol* 9: R137.

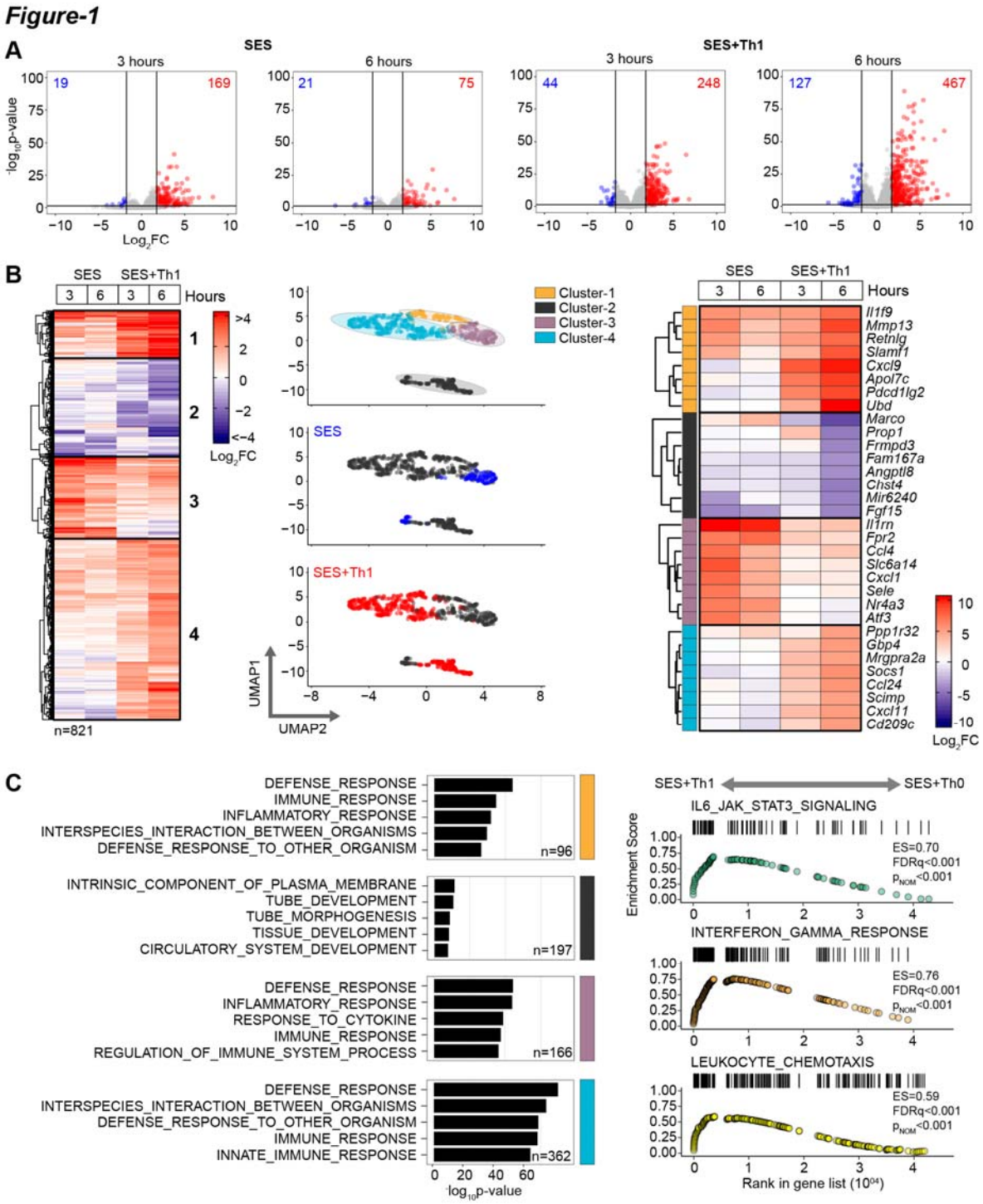

Figure-1. Th1 cells augment the stromal immune response at the expense of tissue homeostasis. (A) RNA-seq was performed on stromal tissues extracted from SES challenged mice. Volcano plots show differential expression analysis (LIMMA) and statistical thresholding (p_{adj}<0.05, Log_2FC>1.75) of datasets obtained at 3 and 6 hours post challenge. Mice were administered (i.p.) with SES alone (SES) or together with Th1-polarised $CD4^+$ T-cells (SES+Th1). Differential expression analysis compares experimental groups with controls; untreated mice

(SES), or mice receiving SES together with naïve $CD4^+$ T-cells (SES+Th0). **(B)** K-means clustering (n=4) of data defined in Panel-A (right-hand heatmap). UMAP visualizations show the distribution of each cluster and their relative involvement in SES (blue) or SES+Th1 (red) driven inflammation. Select examples of genes from each cluster are shown (right-hand heatmap). **(C)** Gene Ontology (msigdb) showcases the top-5 biological processes associated with each cluster (left). Gene set enrichment analysis shows the impact of Th1 cells on Jak-STAT cytokine signalling and leukocyte recruitment. A visualization of the complete GSEA analysis is shown in **Supplemental Figure-1**.

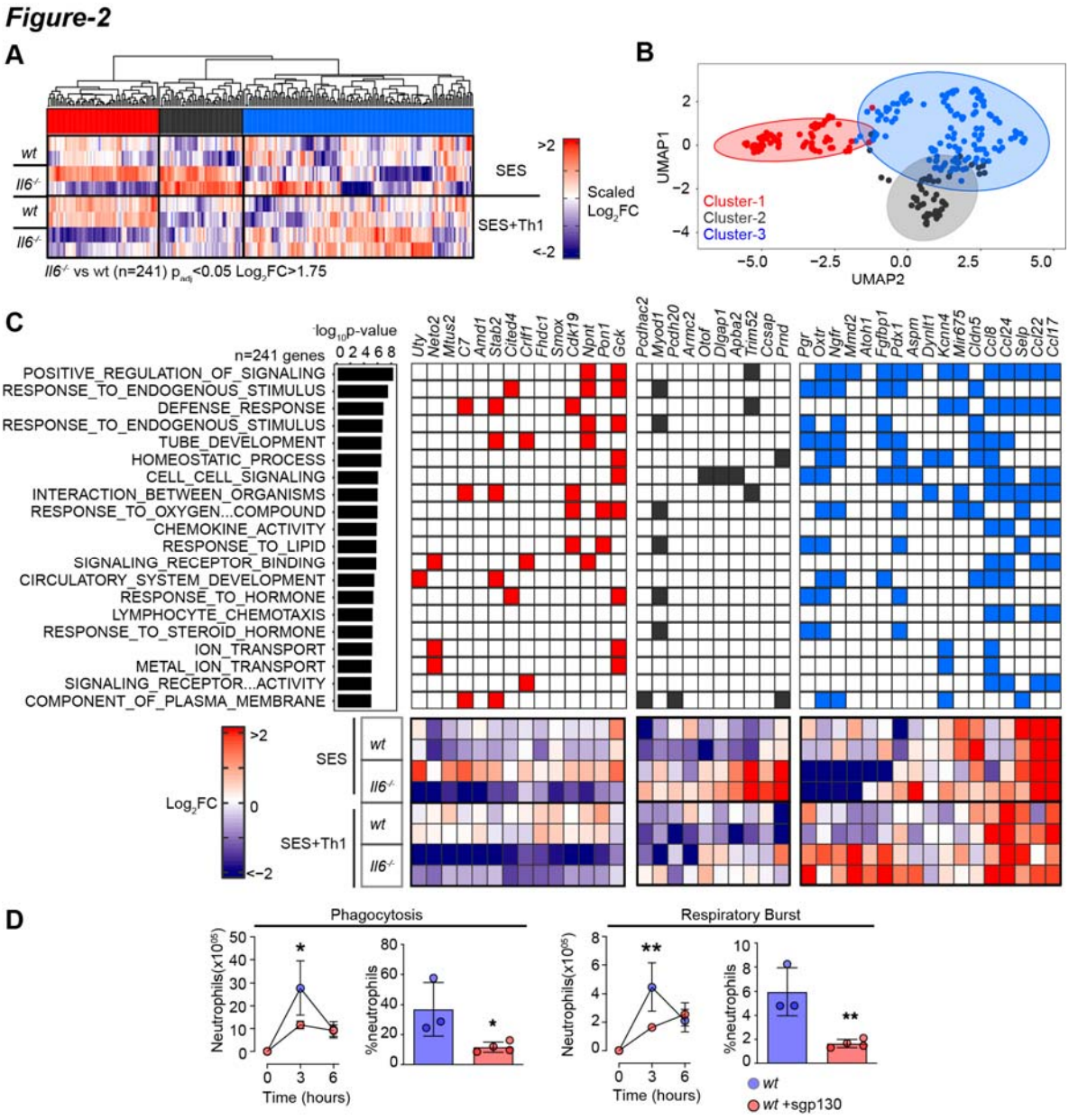

Figure-2. Th1 cells shape the transcriptional output of IL-6. (A) Heatmap of IL-6 regulated transcripts identified by differential expression analysis (LIMMA) of *wt* versus *Il6*$^{-/-}$ mice. Data is arranged by K-means clustering (n=3) of significantly regulated transcripts (Cluster-1; red, Cluster-2; grey, Cluster-3; blue). **(B)** UMAP visualization of all IL-6 regulated transcripts (p_{adj}<0.05, Log_2FC>1.75). **(C)** Alignment of representative transcripts from each Cluster against the top-20 biological processes identified by gene ontology enrichment analysis of 241 IL-6 regulated transcripts (msigdb). **(D)** Flow cytometric analysis of infiltrating neutrophil effector function (see **Supplemental Figure-2**)

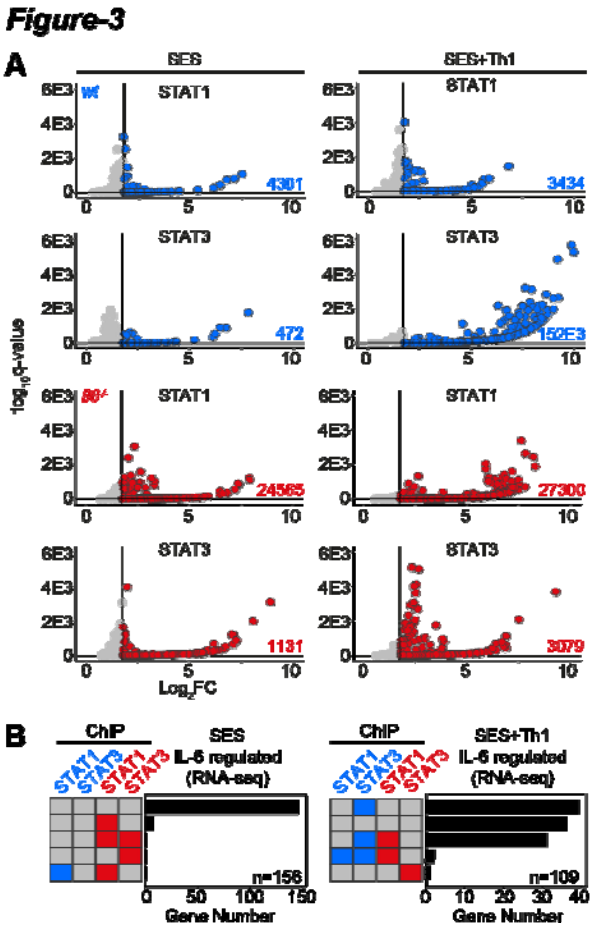

Figure 3. Th1 cells and IL-6 promote a regulatory interplay between STAT1 and STAT3. Chromatin-immunoprecipitation-sequencing (ChIP-seq) of STAT1 and STAT3. Genomic DNA from the peritoneal membrane of mice challenged with SES alone or SES+Th1 was extracted at 3 hours. Peak calling and downstream processing are described in *Materials and Methods*. **(A)** Volcano plots summarize ChIP-seq profiling. Each dot represents a peak (Grey = q>0.05 and/or log_2FC>1.75). Peaks below the significance (q<0.05) and above the log_2FC (>1.75) cutoff values are highlighted blue (*wt*) and red (*Il6*$^{-/-}$). **(B)** STAT transcription factor binding associated with the 241 IL-6 regulated genes identified in Figure-2. Data is separated according to summary data from SES (n=156 genes) and SES+Th1 (109 genes) samples (includes 24 transcripts common to both conditions).

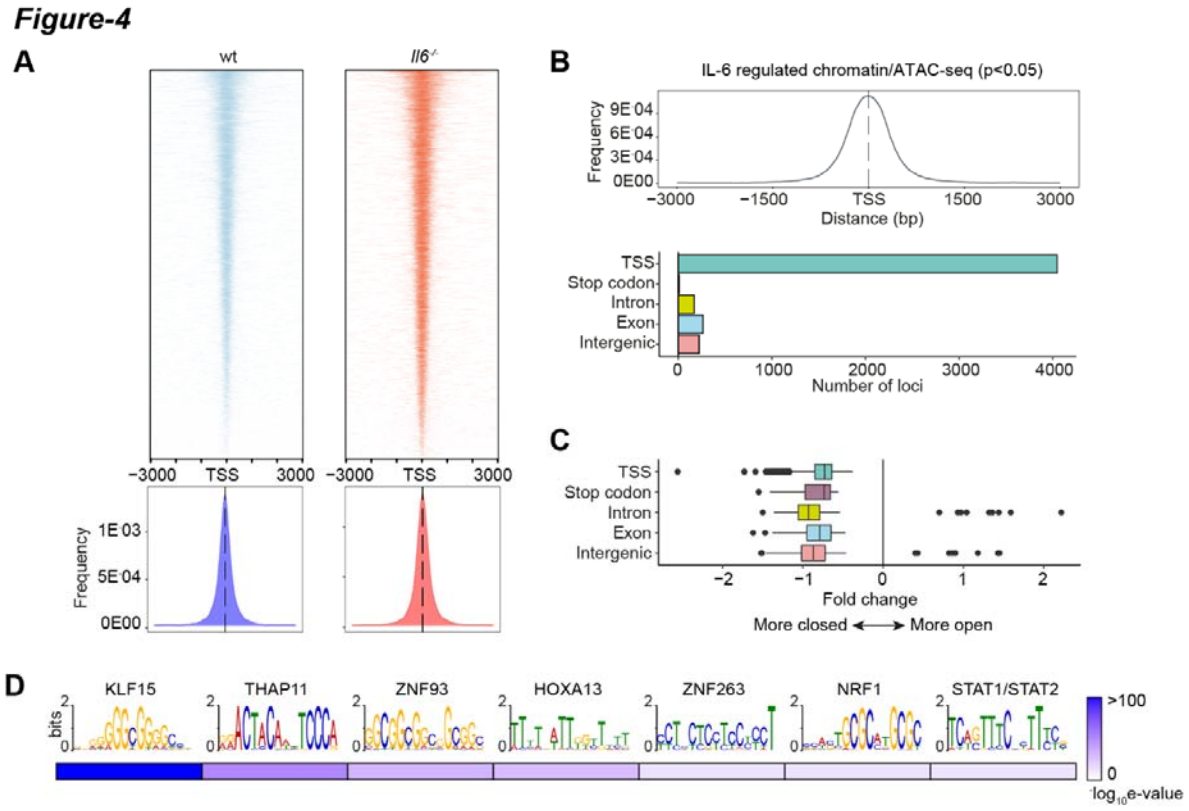

Figure 4. Chromatin accessibility and STAT transcription factor binding. (A) Heatmap visualization of ATAC-seq profiling of peritoneal membrane sections captured from mice treated with SES and Th1 cells (Top). The peak count frequency of sequence reads associated with transcription start sites (TSS) is shown for wt and *Il6*$^{-/-}$ mice (Bottom). **(B)** Histogram shows chromatin accessibility at TSS linked with IL-6 regulated genes (Top). Graph shows the genomic distribution of IL-6 regulated loci (Bottom). **(C)** Fold change (*Il6*$^{-/-}$ vs *wt*) in ATAC-seq reads at indicated genomic features. **(D)** Motif enrichment analysis (MEME-ChIP) of genomic regions identified in differential binding analysis of ATAC-seq datasets. Annotations identify putative transcription factor binding motifs associated with sequencing peaks.

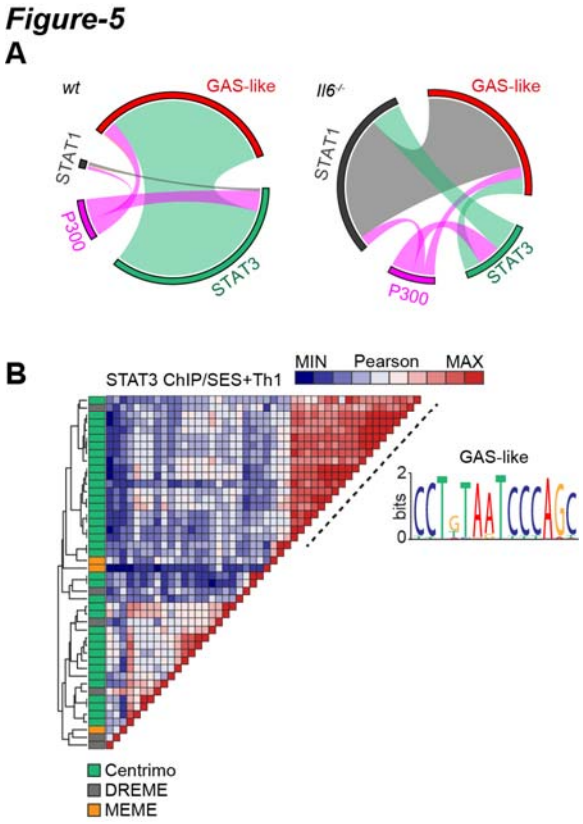

Figure 5. B1 enhancer elements display evidence of STAT1-STAT3 cross-regulation. (A) Circos plots show the relative binding of STAT transcription factors to putative enhancers defined by either P300 binding (either *wt* or *Il6*$^{-/-}$ mice) or sites bearing homology to a *de novo* GAS-like motif identified by STAT1 and STAT3 ChIP-seq (Top). Binding to these sites was calculated using the Bedtools intersect algorithm. **(B)** Motif enrichment analysis of STAT3 ChIP-seq dataset from wt mice (SES+Th1). Pairwise comparison using the Pearson method was generated using Motif Alignment and Search Tool (MAST; Meme ChIP suite). Annotation shows the source algorithm of each motif (Centrimo (green), Meme (orange), and DREME (grey); Meme ChIP suite). A cluster is highlighted (hashed line) that maps to a sequence displaying homology with a GAS-like motif.

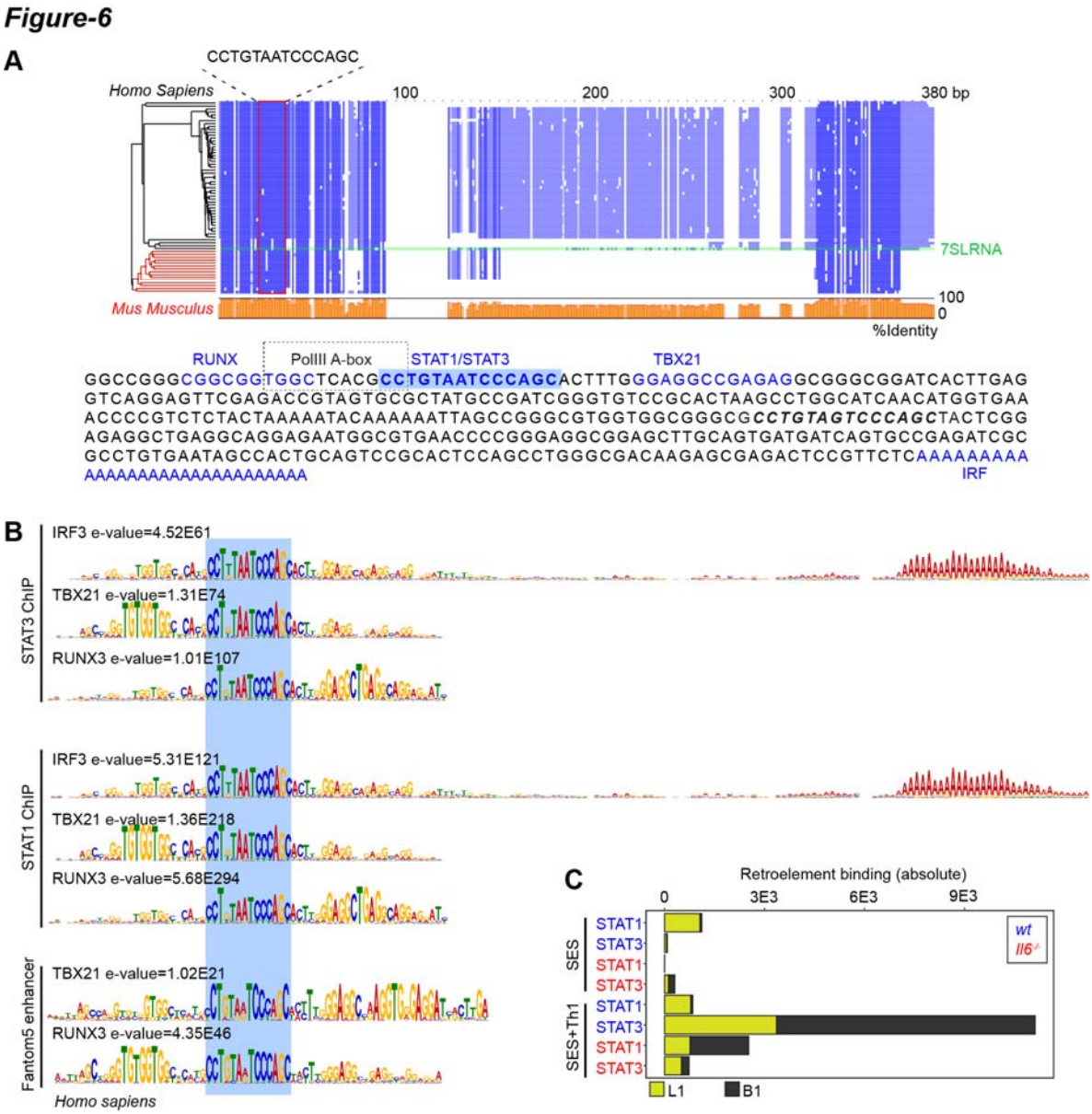

Figure 6. Identification of conserved STAT transcription factor binding motif in Alu elements (A) Multiple sequence alignment (Muscle; EBI) of human and mouse Alu/B1 sequences downloaded from the dfam database (n=66 sequences). The GAS-like motif (CCTGTAATCCCAGC) identified by STAT1 and STAT3 ChIP-seq is located within the sequence. Conserved regions are shown in blue, and a summary of the sequence identity is shown in orange (0-100%). **(B)** Representative secondary motifs (+/-150bp) identified through spaced motif analysis (Spamo; Meme ChIP suite). **(C)** Quantitation of retroelement binding in ChIP datasets based on repeatmasker annotations.

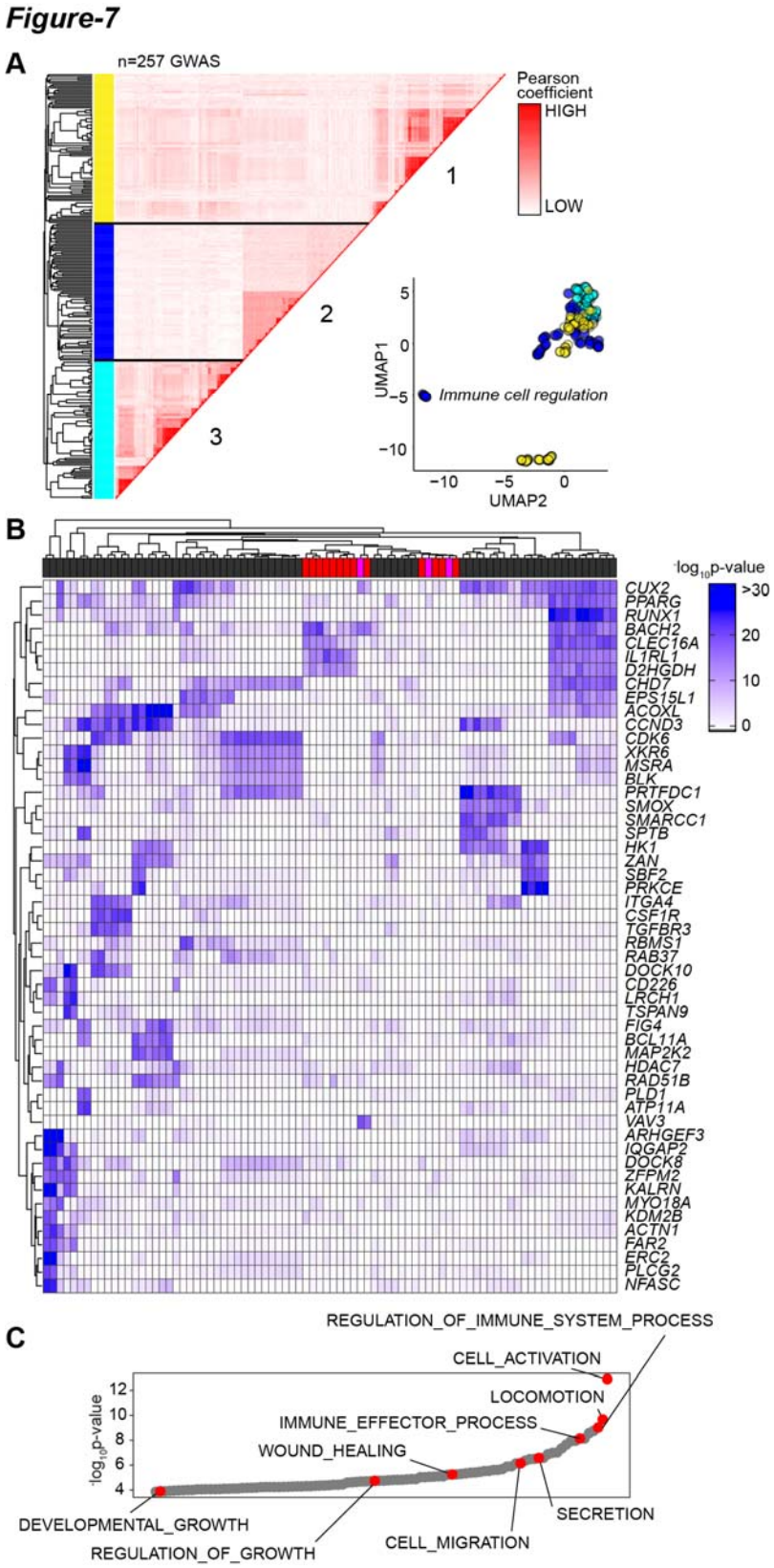

Figure 7. GAS-Alu enhancers associate with human physiology (A) Magma enrichment analysis of motif linked genes identified through enhancer profiling by the Fantom5 consortium. Motif-linked genes

showed significant enrichment for association in 257 GWAS. For each GWAS, a vector was formed of the -log p-values of the motif-linked genes, and Pearson correlations were calculated for each pair of p-value vectors. UMAP distribution identifies a cluster of GWAS related to immune cell function in Cluster-2. **(B)** Top gene-wide p-values identified in Cluster-2 phenotypes. Color bar summarizes GWAS phenotypes linked to immune cell regulation (grey); immunopathology (red); and other (pink). **(C)** Gene Ontology enrichment analysis of the genes identified in Panel-B (n=53).